Identification of Multi-Target Directed Inhibitors of SARS-CoV-2: Drug Repurposing

Yusuf Ayipo
Universiti Sains Malaysia
Waleed Abdullah Ahmad Alananzeh
Universiti Sains Malaysia
NAJIB SANI (najibsani62@student.usm.my)
Universiti Sains Malaysia https://orcid.org/0000-0003-3076-3706
Mohd Mordi
Universiti Sains Malaysia

Research Article

Keywords: SARS-CoV-2, human ACE2, inhibition, computational bioinformatics, antiviral therapy

Posted Date: March 24th, 2021

DOI: https://doi.org/10.21203/rs.3.rs-335733/v1

Abstract

Background: COVID-19 remains a major global challenge while several drugs identified to ameliorate the syndromes are associated with incessant resistance and lack of prospective potentials to permanently curb the infection. This study is aimed at evaluating the potentials of the existing drug molecules to overcome the viral resistance through multi-target inhibition mechanisms.

Methods: Molecular docking and molecular dynamics simulations have been extensively applied to virtually screen 2826 drugs from Selleckem.com library against some key bio-receptors implicated in the SARS-CoV-2 such as the viral nucleocapsid phosphoprotein, the viral spike glycoprotein and the human host ACE2.

Results: Five drugs namely D-(+)-Raffinose pentahydrate (**1**), (-)-Epicatechin gallate (**5**), 2797 (**7**), Rutin DAB10 (**8**) and Hyperoside (**9**) display higher inhibitory potentials against N-terminal NTD of SARS-CoV-2 (PDB 6M3M) with XP docking scores of -16.20, -11.98, -11.83, -11.81 and -11.41 than remdesivir and ribavirin with -10.27 and -9.06 respectively. Their estimated binding free energies against the receptor are -27.80, -27.91, -32.39, -27.91 and -29.50 kcal/mol compared to remdesivir and ribavirin with -24.27 and -15.37 kcal/mol respectively. Similar inhibition patterns were observed against the viral S-protein and the human ACE2 with high stability and bio-functionality.

Conclusion: The identified compounds show promising potentials amenable for breakthrough against the drug-resistant COVID-19 upon further studies.

Introduction

Coronavirus disease 2019 (COVID-19) is a new viral infection of Severe acute respiratory syndrome coronavirus (SARS-CoV-2) which emerged in a suburb city of China towards the end of year 2019 and has spread across countries in all continents of the world. It was later termed COVID-19 pandemic disease by the World Health Organisation (WHO) [1], the situation of which threatens the global health, economy and population severely through daily loss of lives, leading to its further declaration as public health emergency of international concern by WHO in January, 2020 [1, 2]. The death rate of COVID-19 as of 27th August, 2020 stands at 5.0% with 24,331,524 of the global population confirmed infected out of which 16,872,542 patients have recovered and 829,664 [3–5]. The infants and aged population with weak immune systems as well as individuals suffering from co-existing complications of other ailments such as cardiovascular diseases, myocardial injury, hypertension, influenza, diabetes, pneumonia etc are more vulnerable [6–9]. In fact, it's recently reported that not less than 20% and two-thirds mortality in China and Italy respectively had diabetes complication [10]. The age-dependent symptoms of the disease vary from mild such as fever, fatigue, nostril blockage, dry cough, flu-like to Acute respiratory distress syndrome (ARDS), Acute lung injury (ALI), pneumonia, cardiac arrest, dyspnea, liver and kidney damage and death, although asymptomatic cases have been frequently reported [8, 11, 12].

1.1 Structural implications for infection and therapeutic targets

The main pathology still remains elusive [12]. According to virologists, SARS-CoV-2 is a β-CoV family member of *coronaviridae* of the order *Nidovrales,* similar to SARS-CoV-1 and Middle East respiratory syndrome coronavirus (MERS-CoV) [13, 14], with an enveloped single stranded positive ribose nucleic acid (RNA) and crown-like density of proteinous membrane (*corona*) for binding to targets [2]. The structure of SARS-CoV-2 consists of envelope (E) and membrane (M) proteins responsible for structural fusion, spike (S) glycoprotein responsible for cell-interaction with targets and nucleocapsid (N) protein, a viral suppressor protein which resists host defence mechanism and interacts the viral RNA to E, M and S proteins in genome encapsulation (of around 30 000 nucleotides), and the RNA dependent RNA nucleocapsid, a non-structural protein for the viral transcription, virion formation and RNA replication [2, 13, 15]. The highly conserved N-nucleocapsid proteins consist of three main domains, the N-terminal domain (NTD), the central linker rich in serine/arginine and the C-terminal domain (CTD), suggesting them as targets for regulating pathogenic activities [16]. Upon gaining entrance into the host respiratory track, SARS-CoV-2 infuses the host cell in similar way to SARS-CoV-1 and MERS-CoV via the membrane-bound angiotensin-converting enzyme (ACE2) and employs the transmembrane protease serine 2 (TMPRSS2) for S protein activation, the progression of which the viral fusion and replication occur [2, 10, 14]. Although, the possibility of interactions between the viral spike protein and some other human cell adhesion factors such as the dipeptidyl peptidase, cycophillins and ezrin cannot be overruled [17]. Also, sex-dependent epidemiology is possibly observed in the current COVID-19 due to the encoding of ACE2 gene expression on X chromosomes [2], supporting the fact that the signal pathway of the human ACE2 is imperative in the control of COVID-19 infection in addition to the viral S-protein and the nucleocapsid NTD [18–20]. These receptors, nucleocapsid NTD and spike glycoprotein of SARS-CoV-2 are important therapeutic targets and their inhibitors have been clinically experimented in curtailing the pandemic along other angiotensin receptor blockers (ARBs), although, the chance of ACE2 upregulation and altered angiotensin II expression resulting in endothelial dysfunction still a major concern [2, 21].

1.2 Current treatment

The ambiguity surrounding the underlying aetiology of COVID-19 contributes to the scarcity of specific vaccine till moment [11]. In the scientific exploration, WHO recommends the megatrial of various strategies including the repurposing of the existing drugs with different mechanisms such as the antibiotics (e.g. amoxicillin and azithromycin), anti-viral (e.g. ribavirin), anti-CoV (e.g. remdesivir), corticosteroids (methylprednisolone) and antimalarial drugs (chloroquine and its hydroxyl-derivative), using the in-depth relationship in genomic information and pathological features of CoVs [11, 22]. The potential candidates under investigation are classified by inhibition of structural enzymes and proteins responsible for virus-host cells interaction; action on functional proteins and enzymes associated with viral RNA mutation and replication and restoration of human innate immunity (immunomodulation) [11, 23].

The clinical experimental results so far reveal the inhibition of the S-protein and ACE2 by arbidol, the viral nucleocapsid NTD by remdesivir and ribavirin and ACE2 glycosylation by chloroquine analogues [24, 25]. Other conventional medication known for mitigation of ARDS, influenza, ALI, inflammation, hypertension,

immunomodulation have also been evaluated against the pandemic, including losartan, statins and ARBs [2, 26]. Improved immune responses in SARS-CoV and MERS-CoV infected patients have also been investigated upon administration of chemokine and cytokine modulators such as tocilizumab and the human mesenchymal cells [27–29]. However, recurrence of the symptoms due to resistance by the virus, accessibility to all patients and unpleasant side effects are some major challenges with the few drugs in clinical trials of COVID-19 treatment, necessitating the search for new therapeutic candidates with improved pharmacological features and accessibility [21]. Whilst the discovery of novel molecules through the established structural information of the virus seems more promising for a long-term effect but could be costly and untimely, the repositioning of the existing FDA approved drugs is not only cheaper but more appropriate for the situational public-health emergency, even their extended application is very possible. From previous studies, the herbal respiratory detox shot and some other traditional Chinese medicines with known antiviral history were experimented in early prevention and control of COVID-19 through inhibition of SARS-CoV-2's $3CL^{pro}$, PL^{pro}, spike protein etc by theoretical binding and *in vitro* study [1, 30, 31]. Melatonin being a protective agent against some pathogenesis associated with viral infections and ARDS has also been speculated as an adjuvant in the treatment of some chronic ailments induced by COVID-19 including ARDS, ALI and pneumonia [12], supporting the therapeutic potentials of natural products against the pandemic. Since the similarities in pathophysiologies of the existing and emerging CoV strains support the hypothesis of similar pathomechanisms of infection, similar approaches could be rationally employed for their prevention and treatment [14]. The existing drugs with multi-mechanistic inhibitory potentials from abundant natural resources are yet to be extensively explored, as such become viable for this scientific quest.

More so, computational and bioinformatic tools have been extensively applied to understand the cellular factors such as the genome, mutagenesis and amino acid composition of the new Wuhan Seafood market SARS-CoV-2 isolate and predict its transmission and effective therapeutic targets for drug development [32]. Among them, molecular docking and molecular dynamic simulations are important techniques in screening protocols and approximated mimicry of molecular interactions within biocellular environments. Through these applications, some previous studies resulted in the identification of some COVID-19 RdRp and ACE2 potent plant-based inhibitors including hesperidin, sofosbuvir and theaflavin [11, 33, 34], however there exist limited reports on multi-target directed inhibitors of SARS-CoV-2 among the existing FDA-approved drugs. Interestingly, the idea of "one-drug-multiple-targets" are reliable therapeutic strategies for tackling drug resistance and had been successfully employed in previous studies [35–38].

Therefore, this study is aimed at identifying multi-target directed inhibitors of SARS-CoV-2 among the existing drugs through molecular docking and molecular dynamics simulations. The computational tools will be employed to screen 2826 molecules from the drug repurposing library of Selleckchem.com Bioactive compounds expert (https://www.selleckchem.com/screening/drug-repurposing-library.html) against some selected receptor targets implicated in COVID-19 infection and treatment. The crystal structures of the viral nucleocapsid RNA-binding phosphoprotein for RNA mutation and replication of

SARS-CoV-2 (PDB 6M3M), the densely glycosylated S protein for infusion into the human cells (PDB 6VSB) and the human ACE2 for viral reception (PDB 6M17) are carefully selected from RCSB PDB as virtual therapeutic targets for preventing viral translation, mutation, replication and infusion [18, 19, 39]. Theoretical inhibitory potentials against the targets, thermodynamic stability and biological applicability were assessed through molecular docking XP score and molecular dynamic trajectories according to some reported protocols [40–43].

Materials And Methods

2.1 Ligand preparation

The structure data file (SDF) formats of the 2826 drug molecules retrieved from drug repurposing library were imported into the workspace and prepared by Epik energy minimization, followed by the addition of hydrogens, ionization state at pH 7.0 and conversion of 2D to 3D structures. The geometry and partial atomic charges were calculated using Optimized potentials for liquid simulations (OPLS-3e) force field (Schrodinger, 2019-Version LigPrep) [44], the prepared ligands were saved in LigPrep output file.

2.2 Protein preparation

Each PDB file of the selected x-ray structures of the protein targets was pre-processed, optimized by assigning charges and protonation states, refined by deleting water and covalently linked molecules, and moderating the bond order, and regenerating het states using the default Epik pH 7 ± 2. Energy minimization was simulated using OPLS-3e force field in Maestro 12.2 (Schrodinger, 2019-Version Protein Preparation Wizard) [44] followed by removal of non-focused chains.

2.3 Analysis of receptor active cavity and grid box generation

One of the main steps involved in a successful docking simulation is the identification of the active binding site of the receptor target. The active binding sites of the selected receptors were analysed using Biologics site map and sequence alignment modules available in Maestro 12.2 Schrodinger, 2019-version [45], information from the previously reported procedures [18] and available data in the RCSB PDB (https://www.rcsb.org/). The recently released crystal structures of SARS-CoV-2 nucleocapsid phosphoprotein consisting of 499 residues within active chains A, B, C & D, X-ray diffraction resolution of 2.7Å and free R-value of 0.293 (PDB 6M3M), the densely glycosylated S protein consisting of 2904 residues within active chains A, B & C, with electron microscopy resolution of 3.46Å (PDB 6VSB) and the RBD/ACE2-B0AT1 protein complex consisting of 3072 residues within chains A-D with an electron microscopy resolution of 2.90Å were retrieved from the RCSB and submitted to the workspace of Maestro suites one at a time. Each crystal structure was aligned with similarly resolved structures of other CoV strains for binding site comparison using protocols [14, 18] and the Biologics site map function in Maestro [45] predicted five active binding sites (hot-spots) for each with the contributions from the pocket volume, enclosure and hydrophilicity. The binding (druggable) sites were assessed basically with site score and Dscore analysis (eqn. 1 and 2) [46] embedded within the algorithms of Maestro.

Site score = $0.0733n^{½} + 0.6688e – 0.20p$ eqn. (1)

Dscore = $0.094n^{½} + 0.60e – 0.324p$ eqn. (2)

Where n = number of site points; e = enclosure; p = hydrophilic score

The site with highest DScore and consistent configurations with similar reported structures were selected for grid box generation according to the protocols [16, 46]. The active residues within the selected active sites as well as the X, Y and Z coordinates were used to configure the receptor binding grid centroid for docking simulation at 20 Å ligand length. Other parameters are kept at default. In order to validate the predicted binding sites of each receptor and establish the possibility of similar inhibition mechanisms by the drug conformers across different coronavirus strains, the residues of the N-terminal NTD of SARS-CoV-2 nucleocapsid receptor (6M3M) was aligned in sequence with residues of SARS-CoV-1 (PDB 1SSK) and MERS-CoV (PDB 4UD1) of similar targets, while the spike glycoprotein of SARS-CoV-2 (PDB 6VSB) was aligned with the crystal structures representing the same target in SARS-CoV-1 (PDB 6CRX) and MERS-CoV (5W9H).

2.4 Molecular docking

Molecular docking simulations were carried out to estimate the inhibition potential of each minimized conformers of the flexible drug molecules via interactions with the active residues within the generated grid box of each protein target. The results were ranked in increasing order of glide extra precision (XP) scores and binding poses were used to analyse the bonded and non-bonded interactions of the drug molecules with protein residues. The higher the negative value, the stronger the binding.

2.5 Inhibition of SARS-CoV-2 RNA mutation and replication

The prepared conformers of the drugs were virtually screened through algorithms of molecular binding interaction and inhibition potentials against the N protein, NTD of SARS-CoV-2 according to the protocol of [40] incorporating remdesivir and ribavirin as references. The ligands were docked to the crystal structure PDB: 6M3M, within the grid box of the binding site-2 with x, y and z coordinates as 8.08, -7.11 and -30.57 respectively and a default grid space of 1 Å.

2.6 Inhibition of the viral S-protein

The potentials of the drug conformers to inhibit the viral S-protein priming to the human ACE2 were evaluated against the crystal structure of pre-fusion spike glycoprotein of SARS-CoV-2 using docking protocols [41], including remdesivir and ribavirin as references. The single RBD, PDB: 6VSB, within the binding site coordinates x, y and z as 212.56, 211.71 and 224.23 respectively represents the target.

2.7 Blocking of the human ACE2

The abilities of the drugs to block the human ACE2 (host cell) were theoretically evaluated using ligand-receptor docking protocols [42], incorporating remdesivir and ribavirin as references. The crystal structure PDB: 6M17, RBD/ACE2-B0AT1 protein complex within the binding site coordinates x, y and z as 141.53, 141.53 and 202.44 respectively represents the target. The evaluation was based on binding energy in terms of glide XP score, glide energy profiles and bonding and non-bonding interactions are shown by the binding poses. The cumulative results from the docking simulations were used to screen the drug molecules in order to retrieve those with optimum potentials. Since the theoretical biostability and biofunctionalities of a ligand-receptor system cannot be fully established by molecular docking, molecular dynamic simulations were employed for further studies of the selected drugs.

2.8 Molecular dynamics simulations

In order to estimate a more accurate approximations of real biological system mimicry, ligand-receptor complexes of the nine drugs with cumulative highest glide XP gscores and good binding poses were selected for molecular dynamics simulations. The binding affinities, biostabilities, flexibility trajectories and potential systemic functionalities were evaluated in comparison with drugs currently in clinical trial of the COVID-19 treatment, remdesivir and ribavirin. These were achieved through molecular mechanics (MM) force field in Ligand and Receptor Molecular Dynamics server integrated with AMBER 16 force field, CAVER 3.0, Charts.js, ChemAxon, JSmol, MDTraj, MolScript and R (http://chemyang.ccnu.edu.cn/ccb/server/LARMD) [47]. Each ligand-receptor complex was submitted for 'Int-mod' simulation, setting the all-atom MD time at 3000 ps, water explicit and other parameters as default. The average period for each MD simulation ranges between 10 - 25 hours for each drug-receptor system after which the results were retrieved. The average distances between the atoms of the docked ligands as deviated from their original positions were represented by RMSD plots while the radius of gyration plots reveal the root mean square distance between each atom of the protein to their control. The conformational dynamics of each molecular complex system and energetics of the binding ligands were explored by capturing the transition states of the protein receptor with a folding free energy barrier represented by the fractions of native contacts. The fluctuations and isotropic displacements that occurred on each amino acid residue within the period of simulation which denotes the drug-protein stabilities were demonstrated by the RMSF and B-factor plots. Molecular Mechanics Generalized Born Surface Area continuum solvation, MM/GB(SA) re-scoring methods and the statistics of hydrogen bonds between the bound drugs and the protein residues have been used to estimate the binding free energies and affinities between the drug molecules and the residues in the active site of each receptor. The MM/GB(SA) represented by ΔG_{bind} is calculated (eqn. 1-4) [48, 49].

$$\Delta G_{bind} = G_{complex} - G_{receptor} - G_{ligand} \quad \text{eqn. (1)}$$

$$= E_{internal} + EE + VW + GBT + TS \quad \text{eqn. (2)}$$

$$= \Delta H - T\Delta S \approx GE + GBS + TS \quad \text{eqn. (3)}$$

$$GE = GBT - GBS \quad \text{eqn. (4)}$$

Where GE = total gas-phase energy; GBS = GB non-polar contribution to the solvation-accessible surface area; TS = TΔS the entropy contribution by the inhibitor; EE = Electrostatic energy; VW = van der Waals contribution; GBT = GB total; ΔG_{bind} = final binding free energy MM/GB(SA)

The drug molecules with virtually higher inhibitory potentials, biostability and biofunctionalities than the reference drugs, remdesivir and ribavirin were identified and subjected to some biochemical antiviral activity search.

2.9 Antiviral activities of the selected drugs

The selected five (5) drugs from molecular dynamics simulation were traced to some documented biochemical data to find correlation between the theoretical findings in this study and experimental inhibitory actions where possible. Interestingly, all the five have been documented with some pre-clinical and clinical experimental assays *in vitro* and *in vivo* against some virulent viral strains with some similarity in genomic encodings. These include the assay to study inactivation, flocculation and removal of Sindbis virus heat resistant (SVHR) strain in osmolyte solution of drug **1** [50], the inhibition assay of SARS-CoV-1 using quantum dots-conjugated oligonucleotide system for drug **5** [51], the clinical trial on patients infected with hepatitis delta virus (HDV) by administration of 200/400 mg in two doses of drug **7** for 28 days [52], the *in vitro* inhibitory assay on vero cells infected with infectious bronchitis virus (IBV) and the *in vitro* inhibitory assay on murine CoV for drug **8** [51, 53], and the *in vitro* inhibitory assay on human hepatoma Hep G2.2.15 cells, HBeAg and HBsAg, and *in vivo* inhibitory assay on DHBV-DNA-infected duckling model at doses 0.05 g/Kg/day and 0.10 g/Kg/day for drug **9** [54].

3.0 Identification of the selected drugs to their current applications and natural sources

The current applications of the selected drugs as well as their natural product sources were identified using Drug bank and natural plant database (Table 6).

Results And Discussion

4.1 Ligand and protein preparation

A total number of 6834 minimised conformers of the drug molecules were regenerated in a ‘ready-to-dock’ ligprep.out file, while the minimized receptors with binding pocket configurations were prepared in glide_grid.zip files for docking.

4.2 Analysis of receptor active cavity and grid box generation

In line with the set parameters in Maestro, five active sites (hot-spots for ligand binding) were predicted as sites 1-5 with site score, size, Dscore and volume for each receptor in decreasing order of site score (Table 1). The site with the highest predicted Dscore was selected as main target of each receptor. Therefore, site 2, site 1 and site 3 were selected for PDBs 6M3M, 6VSB and 6M17 respectively.

Table 1: Predicted site map parameters for receptor targets

PDB Code	Site	Site score	Size	DScore	Volume
6M3M	1	1.034	621	1.005	2561.18
	2	1.017	194	1.006	618.03
	5	0.605	24	0.599	71.00
	3	0.595	24	0.562	66.20
	4	0.558	23	0.494	92.95
6VSB	3	1.076	836	1.020	2627.38
	1	1.044	1069	1.046	3653.29
	5	1.029	368	1.004	1187.44
	2	1.014	1097	1.031	3739.73
	4	0.996	566	0.938	1439.57
6M17	3	1.029	180	1.042	633.52
	4	1.024	165	0.976	640.04
	2	1.012	186	1.011	658.56
	1	1.012	335	0.956	1383.66
	5	0.991	111	1.034	337.99

The x, y and z grid box coordinated of selected site of each receptor target as well as the potentially active residues for interaction with the drug conformers are presented (Table 2). The site with the highest Dscore in the crystal structure of the N-terminal NTD nucleocapsid phosphoprotein of SARS-COV-2 is site 2 (blue and red cartoon region, Fig. 1A) with the active residue backbones (green labels, Fig. 1B) identifiable within the unique drug targeting site of the NTD terminal (residue numbers 46-174) of the aligned structures of the nucleocapsid proteins of the three CoV strains (Fig. 1C). The residues of SARS-CoV-2 receptors smartly aligned in sequence with the residues of SARS-CoV-1 and MERS-CoV of the same NTD target. Furthermore, the N-terminal NTD SARS-CoV-2 (PDB 6M3M) has 100% homology identity with the resolved structure (PDB 6VYO) (supplementary Fig. 1) whose inhibitors have been demonstrated to be potent against similar targets of other CoV strains. Similarly, the active site of the crystal structure of the viral S glycoprotein of SARS-CoV-2 (PDB 6VSB) (red and blue cartoon, Fig. 1D) reveals the proposed active residues (green labels, Fig. 1E), whose residual sequence aligned smoothly with the resolved active sites for the same target in MERS-CoV (PDB 5W9H) and SARS-CoV-1 (PDB 6CRX) (Fig. 1F). These further validate the possibility of similar inhibition mechanisms by the drug conformers across different coronavirus strains as previously demonstrated [55, 56], and also support the accuracy in the configuration of the binding sites of the receptor targets. The active RBD site as a target for blocking

the host enzyme, ACE2 during infection is mapped (blue and red cartoon, Fig. 1G) with the most probable residues for interaction (green labels, Fig. 1H) traceable to the predictions in Table 2.

Table 2: Predicted binding site properties of the selected structures

PDB code	Site score	Size	DScore	Coordinates			Predicted binding site residues numbers
				X	Y	Z	
6M3M (Site 2)	1.016662	194	1.005915	8.08	-7.11	-30.57	49, 50, 53, 54, 74, 75, 76, 77, 78, 79, 80, 83, 113, 116, 117, 118, 120, 123, 124, 125, 126, 127, 141, 145, 146, 147, 148, 149, 150, 151, 154, 155, 156, 157, 158, 159, 160, 161
6VSB (Site 1)	1.044	1069	1.046	226.32	229.16	206.72	661, 662, 663, 675, 678, 679, 697, 698, 699, 700, 703, 704, 705, 706, 707, 708, 709, 711, 712, 713, 725, 727, 728, 759, 762, 763, 765, 766, 768, 769, 770, 773, 774, 776, 777, 779, 780, 781, 783, 784, 785, 786, 787, 789, 792, 793, 794, 795, 796, 797, 873, 888, 889, 891, 892, 893, 894, 895, 946, 947, 950, 951, 953, 954, 957, 958, 961, 962, 965, 1003, 1005, 1006, 1007, 1009, 1010, 1011, 1012, 1013, 1014, 1015, 1016, 1017, 1018, 1019, 1020, 1021, 1022, 1023, 1024, 1026, 1027, 1028, 1030, 1031, 1034, 1039, 1041, 1042, 1043, 1044, 1045, 1064, 1072, 1074, 1075, 1304, 1309, 1310
6M17	1.029	180	1.042	146.60	201.25	222.83	85, 91, 92, 94, 95, 98, 99, 101, 102, 103, 104, 130, 131, 139, 140, 169, 170, 171, 172, 194, 195, 196, 202, 203, 205, 206, 208, 209, 210, 212, 219, 392, 395, 396, 397, 398, 511, 514, 562, 563, 564, 565, 566, 688, 689, 702, 905

4.3 Protein preparation and receptor grid generation

The active binding pocket grid box of each minimized receptor was generated (in glide grid zip file) for ready-to-dock conformation.

4.4 Molecular docking

The glide XP glide scores, glide energy and binding poses of the nine most interacted drugs across the targets, N-terminal of the RBD of SARS-CoV-2 (PDB 6M3M), S-protein of SARS-CoV-2 (PDB 6VSB) and human ACE2 enzyme (PDB 6M17) are presented presented in Table 3-5. The most strongly interacted drug molecules are buried deep within the binding pocket cavity of each receptor shown by surface structures (Fig. 2). The binding poses to show the bonded and non-bonded residues with the drug molecules within the active site of each receptor as well as the nature of interactions are displayed in Fig. 3-5.

For convenience, the drugs are annotated with numeric identities as given below:

Drug: 1 - S9349 D-(+)-Raffinose pentahydrate

2 - S4768 Melibiose

3 - S3950 Maltitol

4 - S5282 Lactitol monohydrate

5 - S3925 (-)-Epicatechin gallate

6 - S4704 D-(+)-Cellobiose

7 - Drug_Repurposing:2797

8 - Rutin DAB10

9 - S5453 Hyperoside

R1 - Remdesivir

R2 - Ribavirin

Table 3: Docking and molecular dynamic binding free energy of selected drugs with PDB: 6M3M

Drug	Docking scores		Molecular dynamics energy components						
	XP gscore	Glide energy (kcal/mol)	EE	VW	GE	GBS	GBT	TS	MMGB(SA) (kcal/mol)
1	-16.20	-71.96	-23.20	-54.66	-77.86	35.45	-42.40	14.60	-27.80
2	-12.88	-56.47	-14.49	-41.61	-56.10	25.07	-31.04	15.72	-15.32
3	-12.85	-53.03	-18.01	-42.72	-60.73	27.19	-33.54	16.20	-17.34
4	-12.80	-50.92	-11.68	-37.63	-49.31	24.29	-25.02	13.96	-11.06
5	-11.98	-56.52	-16.56	-58.07	-74.63	30.94	-43.69	15.78	-27.91
6	-11.84	-47.11	-17.89	-35.33	-53.22	28.36	-24.86	12.14	-12.72
7	-11.83	-62.03	-18.17	-65.30	-83.47	34.88	-48.59	16.20	-32.39
8	-11.81	-66.16	-16.95	-67.36	-84.31	36.83	-47.48	19.57	-27.91
9	-11.41	-65.26	-26.16	-53.41	-79.56	39.25	-40.32	10.82	-29.50
R1	-10.27	-72.05	-20.34	-62.61	-82.95	36.80	-46.15	21.88	-24.27
R2	-9.06	-41.66	-7.75	-36.76	-44.50	15.01	-29.49	14.12	-15.37

XP = Extra Precision; EE = Electrostatic energy; VW = van der Waals contribution; GE = total gas-phase energy; GBS = GB contribution to solvation; GBT = GB total; MMGB(SA) = final binding free energy. The table is arranged in increasing order of the XP docking scores. For complete table, please refer to the supplementary file.

Considering the inhibition potentials against the viral N-terminal RNA-binding nucleocapsid (PDB: 6M3M) (Table 3), all the drugs including the references interacted with residues within the therapeutic target, NTD region, residue number 46-174 (Fig.1C) of the receptor [18], an indication of inhibitory actions as proposed. Drug **1** has the least XP score followed by **2**, while **9** has the least. In comparison to the reference drugs, **R1** and **R2**, the selected drugs interacted more strongly as indicated by lower glide XP scores. The binding poses (Fig. 3) reveal occupation of the same volume by the selected drugs to the references in favour of common H-bond interactions with similar amino acid residues within the active cavity of the receptor. This predicts conformity in their systemic inhibitory actions. Drug **R1** shows H-bond interactions to Thr A149, Thr D77 and Asn D155 through OH and NH groups respectively similar to **R2** with Thr A149 and Asn B123 through OH groups. The least scored drug **1** interacted with the five amino acid residues through H-bonds, Thr A149, Thr D77, Asn D76, Asn D 78 and Asn B127 all through OH groups while the least scored **9** has four H-bond interactions with Thr A149, Asn D76, Thr A50 and Asn B127, three to OH groups and one to carbonyl O. While all the drugs including the references interacted with Thr A149 through H-bonding and in groups with other residues within the N-terminal NTD, RNA binding domain as resolved [18, 57], only drugs **1, 5** and **9** interacted with Asn B 127, and no bonded

interaction occurred with Trp 53, Ser 79, Hie 146 and Ile 147 along the protein residual chains. The selected ligands displayed similar interactions to the amino acid residues mostly in folds of H-bonding compared to the reference drugs and this favours similar but stronger potential inhibition mechanisms against the mutation and replication of the SARS-CoV-2 RNA along the NTD region.

Table 4: Docking and molecular dynamic binding energy of selected drugs with PDB: 6VSB

Drug	Docking scores		Molecular dynamics energy components						
	XP gscore	Glide energy (kcal/mol)	EE	VW	GE	GBS	GBT	TS	MMGB(SA) (kcal/mol)
1	-12.17	-61.25	-17.39	-68.39	-85.78	31.49	-54.29	17.02	-37.27
2	-11.66	-53.05	-15.21	-47.20	-62.42	25.81	-36.61	19.17	-17.44
7	-11.67	-66.16	-6.81	-65.76	-72.57	22.47	-50.10	20.09	-30.01
4	-11.30	-60.16	-10.59	-45.53	-56.12	17.66	-38.46	19.98	-18.48
3	-10.74	-52.90	-13.42	-43.91	-57.33	22.80	-34.52	19.21	-15.31
8	-10.62	-66.47	-13.56	-69.13	-82.70	28.64	-54.05	19.55	-34.50
5	-10.46	-58.68	-11.97	-62.72	-74.70	23.08	-51.62	23.12	-28.50
9	-10.22	-61.32	-30.63	-64.94	-95.56	36.95	-58.61	20.20	-38.41
6	-9.97	-49.80	-9.44	-44.82	-54.26	18.70	-35.56	23.28	-12.28
R2	-9.10	-43.38	-8.08	-40.48	-48.56	14.37	-34.19	14.45	-19.74
R1	-6.05	-57.95	-6.82	-80.16	-86.98	19.45	-67.52	19.39	-48.13

XP = Extra Precision; EE = Electrostatic energy; VW = van der Waals contribution; GE = total gas-phase energy; GBS = GB contribution to solvation; GBT = GB total; MMGB(SA) = final binding free energy. The table is arranged in increasing order of the XP docking scores. For complete table, please refer to the supplementary file.

The XP docking scores (Table 4) represent the potentials of the selected drugs to inhibit the priming of the SARS-CoV-2 S-protein (PDB 6VSB) to the human ACE2 in comparison with reference drugs in the clinical trial of COVID-19 treatment, remdesivir and ribavirin. Drug **1** shows the best potential in terms of XP docking score followed by **2**, while the least is observed with **6**. However, all the nine selected drugs displayed better interactions, an indication of a more promising potential than the reference drugs. They occupy almost same volume within the binding sub-pocket of the receptor as the references, mostly through H-bond interactions (Fig. 2) and this favours similarity in biological functions. From the binding poses (Fig. 4), **R1** interacted through H-bonds as Asn B1023 and Thr C1027 through H-bonding to OH and

NH group respectively, **R2** show H-bonds through Glu A780, Lys C947, Glu C1017 and Asn A1023, and π – cation to Arg A1019 using OH and NH groups, the best docked drug **1** indicates five H-bond interactions through Asn A1023, Asn B1023, Thr C1027, Arg A1039 and Arg B1039 engaging OH in all. Almost all the drugs including the references interacted with residues number Asn 1023, Thr 1027 and Arg 1039 across different chains, no bonded interaction occurred with Leu 727, Ala 1016, Ser 1021 and Leu 1024 across the residual chains. Interestingly, all the selected drugs including the references interacted with residues within the most important therapeutic targets of the receptor: residues 705-771 in the upstream helix (UH) region, 772-921 in the fusion peptide (FP) region, 922-982 heptad repeat 1 (HR1) region and 983-1028 the central helix (CH) region of the complex spike glycoprotein of SARS-CoV-2 [14, 58]. The selected drugs mostly interacted with more active amino acid residues along various residual chains within the binding pocket of the receptor, an indication of a more promising potential to inhibit the viral S-protein along the therapeutic regions and prevent SARS-CoV-2 infusion to the host than the reference drugs.

Table 5: Docking and molecular dynamic binding energy of selected drugs with PDB: 6M17

Drug	Docking scores		Molecular dynamics energy components						
	XP gscore	Glide energy (kcal/mol)	EE	VW	GE	GBS	GBT	TS	MMGB(SA) (kcal/mol)
8	-12.11	-76.45	-16.48	-65.97	-82.45	32.25	-50.20	37.11	-13.09
1	-11.62	-60.54	-19.18	-54.59	-73.77	31.10	-42.66	33.13	-9.53
5	-10.19	-53.03	-8.76	-54.38	-63.13	20.65	-42.49	31.02	-11.47
2	-9.82	-44.95	-18.34	-45.03	-63.37	28.26	-35.11	32.53	2.58
4	-9.75	-53.50	-21.37	-37.37	-58.73	27.74	-31.00	31.72	0.72
7	-9.58	-63.51	-25.63	-71.44	-97.07	36.44	-60.64	37.70	-22.94
3	-9.20	-45.03	-17.38	-39.56	-56.95	24.62	-32.33	30.17	-2.16
6	-8.91	-44.35	-21.07	-41.48	-62.54	28.53	-34.01	28.68	-5.33
9	-8.26	-42.84	-14.47	-44.81	-59.28	27.97	-31.31	36.02	4.71
R2	-5.96	-36.28	-8.23	-25.67	-33.90	15.11	-18.79	23.02	4.23
R1	-4.64	-60.84	-2.61	-45.70	-48.31	14.08	-34.23	30.65	-3.58

XP = Extra Precision; EE = Electrostatic energy; VW = van der Waals contribution; GE = total gas-phase energy; GBS = GB contribution to solvation; GBT = GB total; MMGB(SA) = final binding free energy. For details, please refer to the supplementary file.

One of the major targets in the vaccination against SARS-CoV-2 infection is the human host cell protease, ACE2. The result (Table 5) shows XP scores as representation of the higher potentials of the selected drugs to block the RBD structure of human ACE2 (PDB 6M17) in comparison with **R1** and **R2**, reference drugs. Drug **8** has the highest potential in terms of glide XP score followed by **1**, while the least is observed in **9**. Interestingly, all the selected nine drugs have lower glide XP scores than the references. The surface and binding poses (Fig. 2 and 5) indicate that all the drugs and the references occupied the same volume and interacted through H-bonding with amino acid residues within the active sub-cavity of the RBD as expected to indicate therapeutic potentials [14]. This could form basis for their similar biological functions. However, as **R1** show three different H-bonding interactions to Asn 194, Glu 208 and Asn 210 through OH and NH groups, **R2** like the selected drugs possesses four H-bond interactions, three through OH to Asp 206, Glu 208 and Lys 562 while the last occur through NH to Asn 210. Drug **8** with the least XP score interacted through six H-bonds (same as drug **1**) between OH at different chemical environment with Glu 98, Tyr 202, Gly 205, Asp 206, Glu 208 and Lys 562 while **9** with the highest score possesses five H-bond interactions through OH to Leu 95, Asp 206, Glu 208, Asn 210 and Lys 652. Residues such as Lys 562, Asn 210 and Glu 208 seems most important at the RBD of the ACE2 receptor as all the drugs including the references strongly interact with them, however, no bonded interactions were formed between the selected drugs and some residues including Ala 99, Tyr 196, Trp 203, Val 209, Leu 392, Gly 395, Ser 511 and Arg 514. All the nine drugs show stronger interactions with similar and more amino acids residues within the catalytic and RBD sites of the ACE2 receptor than the references, an indication of similar but stronger potentials to interfere with the complex (S-protein RBD-ACE2) forming loop region and prevent the infusion of SARS-CoV-2 into the host [19, 42].

4.5 Molecular dynamic simulations

The binding free energies and molecular dynamic trajectories in terms of statistics of H-bond, RMSD, RMSF, Rg and Q plots of the ligand-receptor complex systems of the nine selected drugs are presented in Table 3-5, Fig. 6-8 and supplementary Fig. 2-4.

Molecular dynamics simulation has become an indispensable structural and biophysical tool for an extensive study of biochemical ligand-receptor interactions [59]. From Table 3, the total binding free energy, MMGB(SA) is a sum of GBT and TS which comprehensively quantify the interactions that exist between the small drug molecules and the larger biological target through various conformations. The statistics of H-bond (Fig. 6A) indicates that drugs **8, 5, 1** and **9** possess the highest number of hydrogen bond interactions in descending order, then others along the simulation period. This accounts for their respective higher binding free energy than drugs **2, 4, 6** and **R2** whose number of H-bond interaction occur at lower rates. The RMSD plot (Fig. 6B) shows that the receptor backbone initially experienced slight atomic deviation between 2.0 - 3.5Å and become equilibrated around 1500 ps till the end of simulation with an insignificant deviation of <1.0Å. This indicate that the 3000 ps selected for the simulation is adequate especially since the longer simulations do not necessarily influence the binding free energy and dynamic conformations [60]. The selected drugs mostly entered the equilibrium conditions earlier and maintained it throughout the simulation periods with insignificant deviations in the order **7**<**9**<**1**<**5**<**8**<**R1**.

The dynamic thermal motion paths, transient channels and mean square isotropic displacements which allow the ligands to enter the internal cavities of the receptor are shown by B-factor or temperature factor and RMSF plots (Supplementary Fig. 2C-D). Although all the selected drugs including the references undergo very insignificant fluctuations, however the least is observed in drug **1** and highest in **R2**. These indicate a good thermostability in the drug-receptor systems within the period of simulation. The compactness and stability of the drug-receptor complexes to further probe the structural activity were revealed by the radius of gyration (Rg) plot (Supplementary Fig. 2E). The Rg is influenced by folding state of proteins in a complex with ligands during simulation and it favours drugs **1, 5, 7, 8** and **9** than others including the references. The network of native contacts (Supplementary Fig. 2F) which captures the transition state between the ligands and the receptor with a folding free energy barrier reveal more thermostability of the complexes. A system involving an unfolding protein is indicated by large changes in Q. Thus, selected drugs show better contact with the receptor in folding state along the simulation periods than the references, indicating the flexibility of the receptor to allow stable complexes with the drugs. Cumulatively, drugs **1, 5, 7, 8** and **9** especially show better inhibitory interactions, stability and potent biological functionalities against the target receptor for SARS-CoV-2 RNA replication than **R1** and **R2**.

Drugs **1**, **8** and **9** display higher numbers of H-bond interactions throughout the period of simulation while the least is observed with **R2** (Fig. 7A) consistently with their binding free energy values (Table 4). The RMSD plot (Fig. 7B) indicates that the selected drugs, the references as well as the receptor backbone form stable systems with little or no deviation of atom/residue throughout the period of simulation. In spite of this, the least fluctuation is observed in **1** and **2** while **R1** and **R2** produced the largest during the thermodynamic simulation as shown (Supplementary Fig. 3C-D). The receptor enters into a folding state with drugs **1** and **8** the most during the simulation while the least is observed with **R1** and **R2** (Supplementary Fig. 3E), although all the drugs including the references favour the folding of the receptor except **4** as indicated (Supplementary Fig. 3F). On the average, the selected drugs display virtual inhibitory potentials, stability and bio-applicability in complex with the receptor representing the viral spike glycoprotein.

The plot of statistics of H-bond interactions throughout the simulation trajectory (Fig. 8A) indicates that drugs **7, 8** and **9** have the highest number while drug **4** show the least consistently with their binding free energy scores (Table 5). Others considerably compete with **R1** and **R2**. The RMSD plot (Fig. 8B) reveals that the receptor backbones become stable around 1300 ps, and only undergoing an insignificant fluctuation of <1Å till the end of simulation while the drugs including the references form stable systems almost throughout the period of simulation (Supplementary Fig. 4C-D). Although the compactness, protein folding state and stability (Supplementary Fig. 4E-F) favour all the drugs including the references in complex with the receptor, however a little deviation is observed in **R2**. Summarily the drugs virtually interact more strongly and form stable systems with the receptor, an indication of potential abilities to actively block the human ACE2 against SARS-CoV-2 infection in better forms than the reference drugs.

4.6 Biochemical analysis of the antiviral activities of the selected drugs

The selected drugs coincidentally have been experimented for efficacy against some virulent viral strains through anti-CoV/antiviral activities and the results (Table 6) indicate potent inhibition. From the biochemical analysis, the drugs demonstrate strong inhibitory activity *in vitro* and *in vivo* experimental models including clinical trials against some coronaviruses and other virulent viral strains, corroborating the theoretical findings presented above. Their mechanisms of antiviral actions include prevention of viral infusion, disruption of viral E proteins, inhibition of prenylation, disruption of the viral RNA for replication, inhibition of viral DNA and suppression of enteroviruses [50–54]. This phenomenon is reasonably feasible due to some degrees of genomic similarities that exist among active pathogenic sites of the viral strains [61]. Advantages of repurposing already approved drugs for this quest include the availability of physico-chemical and pharmacodynamics information as well as documented activity data relevant to the study, additionally supporting the promising inhibition in real biological system.

Table 6: Biochemical *in vitro* and *in vivo* experimental results on the inhibition of the selected drugs against CoVs/other viral strains

Drug	Experimental protocol	Result	Ref.
1	Inactivation, flocculation and removal of SVHR strain in osmolyte solution of the drug.	>90% flocculation and removal of SVHR occurred at concentration range of 0.3-1.0 M.	[50]
5	Inhibition assay of SARS-CoV-1 using quantum dots-conjugated oligonucleotide system	Dose-dependent inhibition >40% at 0.05 µg/mL observed with IC_{50} = 0.05 µg/mL.	[51]
7	Clinical trial on patients infected with HDV by administration of 200/400 mg in two doses for 28 days.	HDV-RNA declined by 0.73 log and 1.54 log at low and high doses respectively. This is significantly higher than the effect of placebo.	[52]
8	*In vitro* inhibitory assay on Vero cells infected with IBV; *In vitro* inhibitory assay on murine CoV	Inhibits the viral replication in dose-dependents up to 4-6-folds titer reduction at 0.004 g/mL of crude extract rich in drug **8**. Inhibition of murine CoV occur at concentration range of 15.63-500 µg/mL	[51, 53]
9	*In vitro* inhibitory assay on human hepatoma Hep G2.2.15 cells, HBeAg and HBsAg. *In vivo* inhibitory assay on DHBV-DNA-infected duckling model at doses 0.05 g/Kg/day and 0.10 g/Kg/day	Significant inhibition with TC_{50} = 0.115g/L and maximum TC_0 = 0.05g/L. The IC_{50}s for HBeAg and HBsAg are 0.012 g/L and 0.015 g/L after 4-day, 0.009 g/L and 0.011 g/L after 8-day treatment respectively. Great reduction in DHBV-DNA (*p<0.01*) with mean percentage of viral DNA inhibition as 56.24% and 60.94% for 0.05 g/Kg/day and 0.10 g/Kg/day respectively.	[54]

4.7 Identification of the selected drugs to their current applications and natural sources

The information presented in Table 7 indicate that the five (5) selected drugs (Scheme 1) are either currently approved for clinical trials or in use for treatment of some ailments. More interestingly, they are commercially available and mostly traceable to vastly available natural products. This study thus, demonstrates their dual applicability potentials.

Table 7: Selected drugs, their current clinical applications and natural sources

Drug	Current application	Sources
1	In clinical trial for cardiovascular disease	*Eucalyptus spp, Myrtaceae,* cotton seed meal
5	Investigated for treatment of hypertension and pre-diabetes	*Camellia sinensis* (green tea plant)
7	In trial study for treating solid tumour, lung cancer and leukemia	Synthetic
8	Used to treat capillary fragility	*Forsythia, Hydrangea, Viola,* buckwheat, tobacco
9	Hepatoprotective and metabolic agent	*Agrimonia eupatoria, Arctostaphylos uva-ursi, Hypericum perforatum, Crataegus laevigata, Crataegus monogyna, Fagopyrum esculentum, Houttuynia cordata, Polygonum multiflorum, Tussilago farfara, Rosa canina, Rumex acetosa, Artemisia capillaris*

Similar to other previously reported study [40–43], the application of computational tools such as molecular docking and molecular dynamics simulation have afforded fast and cheap demonstration of multi-target directed inhibition mechanisms against SARS-CoV-2 through the viral N-terminal NTD nucleocapsid phosphoprotein for translation and replication, the viral S protein along its various therapeutic targets for infusion and the human ACE2 to reception. The molecular docking protocols reveal that the drugs show stronger inhibition potentials against the targets than remdesivir and ribavirin, drugs in clinical trials. The molecular dynamics simulations to approximately mimic the real biological system also indicate better binding affinity, biostability and biofunctionalities in favour of the selected drugs than the references. Interestingly, the drugs have activity history which corroborate the findings from the virtual studies. The selected drugs were also traced to abundant natural resources for global accessibility. The protocols reveal that the identified drugs possess stronger multi-target inhibition potentials against the SARS-CoV-2 pathogenic targets, similarly to some previous studies where multi-target inhibition mechanisms have been demonstrated in favour of some bioactive agents against cancer-related targets/pathways to overcome incessant resistance to drugs [62, 63].

Conclusion

The rigorous molecular simulations adopted in this research work have aided the identification of potential inhibitors of various targeted human/viral enzymes and protein receptors implicated in SARS-CoV-2 infection such as the human ACE2, the viral spike glycoprotein and the viral nucleocapsid protein

than the remdesivir and ribavirin previously reported. The five drugs for various applications from Selleckem.com drug repurposing library (Table V), D-(+)-Raffinose pentahydrate (**1**), (-)-Epicatechin gallate (**5**), 2797 (**7**), Rutin DAB10 (**8**) and Hyperoside (**9**) have virtually demonstrated higher inhibitory potentials, stabilities and biological functionalities through different mechanisms against the selected therapeutic targets than the references. Their biological activities against some virulent viral strains including SARS-CoV-1 and murine CoV previously documented are consistent with the theoretical findings in this study, a strong promise of bona fide inhibition against SARS-CoV-2. Interestingly, their commercial availability and presence in natural products (in measurable amounts) could enhance the global research-based developmental studies in the discovery of effective therapeutic candidates against the pandemic. Although, the study requires computing resources and more efficient algorithms for accurate and comprehensive understanding of real biological processes, common to computational approaches in drug design, and more robust biochemical analysis targeting specifically SARS-CoV-2 is required to further affirm the potentials of the drugs as bona fide inhibitors, however, it presents a model amenable for further studies towards designing more effective and accessible therapeutic candidates, acting through multi-target mechanisms to overcome the incessant drug resistance associated with the pandemic COVID-19.

Declarations

Conflict of interest

No conflict of interest was declared in the research.

Acknowledgement

This work was supported by Ministry of Higher Education of Malaysia, HICoE (grant no. 311/CDADAH/4401009). Ayipo Y. O. wishes to acknowledge the Tertiary Education Fund, Nigeria and Kwara State University Malete Nigeria for PhD Sponsorship and Universiti Sains Malaysia GA Scheme (grant no. 308.AIPS.415401).

Author Contributions

Sani Najib Yahaya, Yusuf Oloruntoyin Ayipo, Thenmoly Damodaran, and Mohd Nizam Bn Mordi all contributed to the review and drafted the paper. All authors provided revisions of the paper and have approved the final manuscript. Sani Najib and Yusuf Ayipo developed the manuscript, while Thenmoly Damodaran and Mohd Nizam critiqued the included papers and reviewed the manuscripts.

Consent to Participate (Ethics)

All authors have full consent to participate in writing this manuscript

Consent to Publish (Ethics)

Authors declared consent to publish this manuscript

References

1. Zhang Z, Wu W, yong, Hou J jun, et al (2020) Active constituents and mechanisms of Respiratory Detox Shot, a traditional Chinese medicine prescription, for COVID-19 control and prevention: Network-molecular docking-LC–MSE analysis. J Integr Med 18:229–241. https://doi.org/10.1016/j.joim.2020.03.004
2. Atri D, Siddiqi HK, Lang JP et al (2020) COVID-19 for the Cardiologist: Basic Virology, Epidemiology, Cardiac Manifestations, and Potential Therapeutic Strategies. JACC Basic to Transl Sci 5:518–536. https://doi.org/10.1016/j.jacbts.2020.04.002
3. Abel R, Mondal S, Masse C et al (2017) Accelerating drug discovery through tight integration of expert molecular design and predictive scoring. Curr Opin Struct Biol 43:38–44. https://doi.org/10.1016/j.sbi.2016.10.007
4. Akram M, Waratchareeyakul W, Haupenthal J et al (2017) Pharmacophore modeling and in Silico/in Vitro screening for human cytochrome P450 11B1 and cytochrome P450 11B2 inhibitors. Front Chem 5:1–14. https://doi.org/10.3389/fchem.2017.00104
5. AL-Refaei MA, Makki RM, Ali HM (2020) Structure prediction of transferrin receptor protein 1 (TfR1) by homology modelling, docking, and molecular dynamics simulation studies. Heliyon 6:e03221. https://doi.org/10.1016/j.heliyon.2020.e03221
6. Fang L, Karakiulakis G, Roth M (2020) Antihypertensive drugs and risk of COVID-19? – Authors' reply. Lancet Respir Med 8:e32–e33. https://doi.org/10.1016/S2213-2600(20)30159-4
7. Guo T, Fan Y, Chen M et al (2020) Cardiovascular Implications of Fatal Outcomes of Patients with Coronavirus Disease 2019 (COVID-19). JAMA Cardiol 5:811–818. https://doi.org/10.1001/jamacardio.2020.1017
8. Gupta R, Ghosh A, Singh AK, Misra A (2020) Clinical considerations for patients with diabetes in times of COVID-19 epidemic. Diabetes Metab Syndr Clin Res Rev 14:211–212. https://doi.org/10.1016/j.dsx.2020.03.002
9. Gupta R, Misra A (2020) Contentious issues and evolving concepts in the clinical presentation and management of patients with COVID-19 infectionwith reference to use of therapeutic and other drugs used in Co-morbid diseases (Hypertension, diabetes etc). Diabetes Metab Syndr Clin Res Rev 14:251–254. https://doi.org/10.1016/j.dsx.2020.03.012
10. Hoffmann M, Kleine-Weber H, Schroeder S et al (2020) SARS-CoV-2 Cell Entry Depends on ACE2 and TMPRSS2 and Is Blocked by a Clinically Proven Protease Inhibitor. Cell 181:271–280.e8. https://doi.org/10.1016/j.cell.2020.02.052
11. Wu C, Liu Y, Yang Y et al (2020) Analysis of therapeutic targets for SARS-CoV-2 and discovery of potential drugs by computational methods. Acta Pharm Sin B 10:766–788. https://doi.org/10.1016/j.apsb.2020.02.008
12. Zhang R, Wang X, Ni L et al (2020) COVID-19: Melatonin as a potential adjuvant treatment. Life Sci 250:117583. https://doi.org/10.1016/j.lfs.2020.117583

13. Elfiky AA (2020) Anti-HCV, nucleotide inhibitors, repurposing against COVID-19. Life Sci 248:117477. https://doi.org/10.1016/j.lfs.2020.117477
14. Xia S, Liu M, Wang C et al (2020) Inhibition of SARS-CoV-2 (previously 2019-nCoV) infection by a highly potent pan-coronavirus fusion inhibitor targeting its spike protein that harbors a high capacity to mediate membrane fusion. Cell Res 30:343–355. https://doi.org/10.1038/s41422-020-0305-x
15. Kannan S, Ali Pakeer PSS, Ali AS, Hemalatha K (2020) Reply Letter - COVID-19 (Novel Coronavirus 2019) - Recent trends. Eur Rev Med Pharmacol Sci 24:6482–6483. https://doi.org/10.26355/eurrev_202006_21629
16. Yadav R, Imran M, Dhamija P et al (2020) Virtual screening and dynamics of potential inhibitors targeting RNA binding domain of nucleocapsid phosphoprotein from SARS-CoV-2. J Biomol Struct Dyn 0:1–16. https://doi.org/10.1080/07391102.2020.1778536
17. Vankadari N, Wilce JA (2020) Emerging WuHan (COVID-19) coronavirus: glycan shield and structure prediction of spike glycoprotein and its interaction with human CD26. Emerg Microbes Infect 9:601–604. https://doi.org/10.1080/22221751.2020.1739565
18. Kang S, Yang M, Hong Z et al (2020) Crystal structure of SARS-CoV-2 nucleocapsid protein RNA binding domain reveals potential unique drug targeting sites. Acta Pharm Sin B 10:1228–1238. https://doi.org/10.1016/j.apsb.2020.04.009
19. Wrapp D, Wang N, Corbett KS et al (2020) Cryo-EM structure of the 2019-nCoV spike in the prefusion conformation. bioRxiv 1263:1260–1263. https://doi.org/10.1101/2020.02.11.944462
20. Wu D, Yang XO (2020) TH17 responses in cytokine storm of COVID-19: An emerging target of JAK2 inhibitor Fedratinib. J Microbiol Immunol Infect 53:368–370. https://doi.org/10.1016/j.jmii.2020.03.005
21. Fedson DS, Opal SM, Rordam OM (2020) Hiding in plain sight: An approach to treating patients with severe covid-19 infection. MBio 11:1–3. https://doi.org/10.1128/mBio.00398-20
22. Kupferschmidt K, Cohen J (2020) Race to find COVID-19 treatments accelerates. Science 367:1412–1413. https://doi.org/10.1126/science.367.6485.1412
23. Scalise M, Indiveri C (2020) Repurposing Nimesulide, a Potent Inhibitor of the B0AT1 Subunit of the SARS-CoV-2 Receptor, as a Therapeutic Adjuvant of COVID-19. SLAS Discov 25:1171–1173. https://doi.org/10.1177/2472555220934421
24. Liu C, Zhou Q, Li Y et al (2020) Research and Development on Therapeutic Agents and Vaccines for COVID-19 and Related Human Coronavirus Diseases. ACS Cent Sci 6:315–331. https://doi.org/10.1021/acscentsci.0c00272
25. Liu T, Luo S, Libby P, Shi GP (2020) Cathepsin L-selective inhibitors: A potentially promising treatment for COVID-19 patients. Pharmacol Ther 213:107587. https://doi.org/10.1016/j.pharmthera.2020.107587
26. Phadke M, Saunik S (2020) COVID-19 treatment by repurposing drugs until the vaccine is in sight. Drug Dev Res 81:541–543. https://doi.org/10.1002/ddr.21666

27. Bennardo F, Buffone C, Giudice A (2020) New therapeutic opportunities for COVID-19 patients with Tocilizumab: Possible correlation of interleukin-6 receptor inhibitors with osteonecrosis of the jaws. Oral Oncol 106:104659. https://doi.org/10.1016/j.oraloncology.2020.104659
28. Ceribelli A, Motta F, De Santis M et al (2020) Recommendations for coronavirus infection in rheumatic diseases treated with biologic therapy. J Autoimmun 109:102442. https://doi.org/10.1016/j.jaut.2020.102442
29. Shetty AK (2020) Mesenchymal stem cell infusion shows promise for combating coronavirus (COVID-19)-induced pneumonia. Aging Dis 11:462–464. https://doi.org/10.14336/AD.2020.0301
30. Yang Y, Islam MS, Wang J et al (2020) Traditional Chinese medicine in the treatment of patients infected with 2019-new coronavirus (SARS-CoV-2): A review and perspective. Int J Biol Sci 16:1708–1717. https://doi.org/10.7150/ijbs.45538
31. Zhang D, Wu K, Zhang X et al (2020) In silico screening of Chinese herbal medicines with the potential to directly inhibit 2019 novel coronavirus. J Integr Med 18:152–158. https://doi.org/10.1016/j.joim.2020.02.005
32. Robson B (2020) Computers and viral diseases. Preliminary bioinformatics studies on the design of a synthetic vaccine and a preventative peptidomimetic antagonist against the SARS-CoV-2 (2019-nCoV, COVID-19) coronavirus. Comput Biol Med 119:103670. https://doi.org/10.1016/j.compbiomed.2020.103670
33. Elfiky AA (2020) Anti-HCV, nucleotide inhibitors, repurposing against COVID-19. Life Sci 248:. https://doi.org/10.1016/j.lfs.2020.117477
34. Lung J, Lin YS, Yang YH et al (2020) The potential chemical structure of anti-SARS-CoV-2 RNA-dependent RNA polymerase. J Med Virol 92:693–697. https://doi.org/10.1002/jmv.25761
35. Joshi RS, Jagdale SS, Bansode SB et al (2020) Discovery of potential multi-target-directed ligands by targeting host-specific SARS-CoV-2 structurally conserved main protease. J Biomol Struct Dyn 0:1–16. https://doi.org/10.1080/07391102.2020.1760137
36. Kadioglu O, Saeed M, Greten HJ, Efferth T (2020) Identification of novel compounds against three targets of SARS CoV2 coronavirus by combined virtual screening and supervised machine learning. Bull World Heal Organ 1–29
37. Mansour MA, Aboulmagd AM, Abdel-Rahman HM (2020) Quinazoline-Schiff base conjugates:: In silico study and ADMET predictions as multi-target inhibitors of coronavirus (SARS-CoV-2) proteins. RSC Adv 10:34033–34045. https://doi.org/10.1039/d0ra06424f
38. Murugan NA, Kumar S, Jeyakanthan J, Srivastava V (2020) Searching for target-specific and multi-targeting organics for Covid-19 in the Drugbank database with a double scoring approach. Sci Rep 10:1–16. https://doi.org/10.1038/s41598-020-75762-7
39. Yan R, Zhang Y, Guo Y et al (2020) Structural basis for the recognition of the 2019-nCoV by human ACE2. 2762:1–10. https://doi.org/10.1101/2020.02.19.956946
40. Bhowmik D, Nandi R, Jagadeesan R et al (2020) Identification of potential inhibitors against SARS-CoV-2 by targeting proteins responsible for envelope formation and virion assembly using docking

based virtual screening, and pharmacokinetics approaches. Infect Genet Evol 84:104451. https://doi.org/10.1016/j.meegid.2020.104451

41. Sinha SK, Shakya A, Prasad SK et al (2020) An in-silico evaluation of different Saikosaponins for their potency against SARS-CoV-2 using NSP15 and fusion spike glycoprotein as targets. J Biomol Struct Dyn 0:000. https://doi.org/10.1080/07391102.2020.1762741
42. Vardhan S, Sahoo SK (2020) In silico ADMET and molecular docking study on searching potential inhibitors from limonoids and triterpenoids for COVID-19. Comput Biol Med 124:103936. https://doi.org/10.1016/j.compbiomed.2020.103936
43. Yu R, Chen L, Lan R et al (2020) Computational screening of antagonists against the SARS-CoV-2 (COVID-19) coronavirus by molecular docking. Int J Antimicrob Agents 56:106012. https://doi.org/10.1016/j.ijantimicag.2020.106012
44. Jorgensen WL, Maxwell DS, Tirado-Rives J (1996) Development and testing of the OPLS all-atom force field on conformational energetics and properties of organic liquids. J Am Chem Soc 118:11225–11236. https://doi.org/10.1021/ja9621760
45. TA H (2009) Identifying and characterizing binding sites and assessing druggability. J Chem Inf Model 49:377–389
46. Vidler LR, Brown N, Knapp S, Hoelder S (2012) Druggability analysis and structural classification of bromodomain acetyl-lysine binding sites. J Med Chem 55:7346–7359. https://doi.org/10.1021/jm300346w
47. Yang JF, Wang F, Chen YZ et al (2020) LARMD: Integration of bioinformatic resources to profile ligand-driven protein dynamics with a case on the activation of estrogen receptor. Brief Bioinform 21:2206–2218. https://doi.org/10.1093/bib/bbz141
48. Priya P, Kesheri M, Sinha RP, Kanchan S (2015) Molecular Dynamics Simulations for Biological Systems
49. Karplus M, Petsko GA (1990) Molecular dynamics simulations in biology. Nature 347:631–639. https://doi.org/10.1038/347631a0
50. Gencoglu MF, Heldt CL (2015) Enveloped virus flocculation and removal in osmolyte solutions. J Biotechnol 206:8–11. https://doi.org/10.1016/j.jbiotec.2015.03.030
51. Annunziata G, Sanduzzi Zamparelli M, Santoro C et al (2020) May Polyphenols Have a Role Against Coronavirus Infection? An Overview of in vitro Evidence. Front Med 7:1–7. https://doi.org/10.3389/fmed.2020.00240
52. Rizzetto M, Ciancio A (2015) The prenylation inhibitor, lonafarnib: A new therapeutic strategy against hepatitis delta. Lancet Infect Dis 15:1119–1120. https://doi.org/10.1016/S1473-3099(15)00155-3
53. Islam MT, Sarkar C, El-Kersh DM et al (2020) Natural products and their derivatives against coronavirus: A review of the non-clinical and pre-clinical data. Phyther Res 34:2471–2492. https://doi.org/10.1002/ptr.6700
54. Wu LL, Yang XB, Huang ZM et al (2007) In vivo and in vitro antiviral activity of hyperoside extracted from Abelmoschus manihot (L) medik. Acta Pharmacol Sin 28:404–409.

https://doi.org/10.1111/j.1745-7254.2007.00510.x

55. Brown AJ, Won JJ, Graham RL et al (2019) Broad spectrum antiviral remdesivir inhibits human endemic and zoonotic deltacoronaviruses with a highly divergent RNA dependent RNA polymerase. Antiviral Res 169:104541. https://doi.org/10.1016/j.antiviral.2019.104541
56. Calligari P, Bobone S, Ricci G, Bocedi A (2020) Molecular investigation of SARS–COV-2 proteins and their interactions with antiviral drugs. Viruses 12:. https://doi.org/10.3390/v12040445
57. Dinesh DC, Chalupska D, Silhan J et al (2020) Structural basis of RNA recognition by the SARS-CoV-2 nucleocapsid phosphoprotein. PLoS Pathog 16:. https://doi.org/10.1371/journal.ppat.1009100
58. Mercurio I, Tragni V, Busto F et al (2020) Protein structure analysis of the interactions between SARS-CoV-2 spike protein and the human ACE2 receptor: from conformational changes to novel neutralizing antibodies. Cell Mol Life Sci. https://doi.org/10.1007/s00018-020-03580-1
59. Lynch DL, Hurst DP, Shore DM et al (2017) Molecular Dynamics Methodologies for Probing Cannabinoid Ligand/Receptor Interaction, 1st ed. Elsevier Inc
60. Jiménez-Alberto A, Ribas-Aparicio RM, Aparicio-Ozores G, Castelán-Vega JA (2020) Virtual screening of approved drugs as potential SARS-CoV-2 main protease inhibitors. Comput Biol Chem 88:107325. https://doi.org/10.1016/j.compbiolchem.2020.107325
61. Chang CK, Hou MH, Chang CF et al (2014) The SARS coronavirus nucleocapsid protein - Forms and functions. Antiviral Res 103:39–50. https://doi.org/10.1016/j.antiviral.2013.12.009
62. Skok Ž, Zidar N, Kikelj D, Ilaš J (2020) Dual Inhibitors of Human DNA Topoisomerase II and Other Cancer-Related Targets. J Med Chem 63:884–904. https://doi.org/10.1021/acs.jmedchem.9b00726
63. Zilbermintz L, Leonardi W, Tran SH et al (2016) Cross-inhibition of pathogenic agents and the host proteins they exploit. Sci Rep 6:1–9. https://doi.org/10.1038/srep34846

Figures

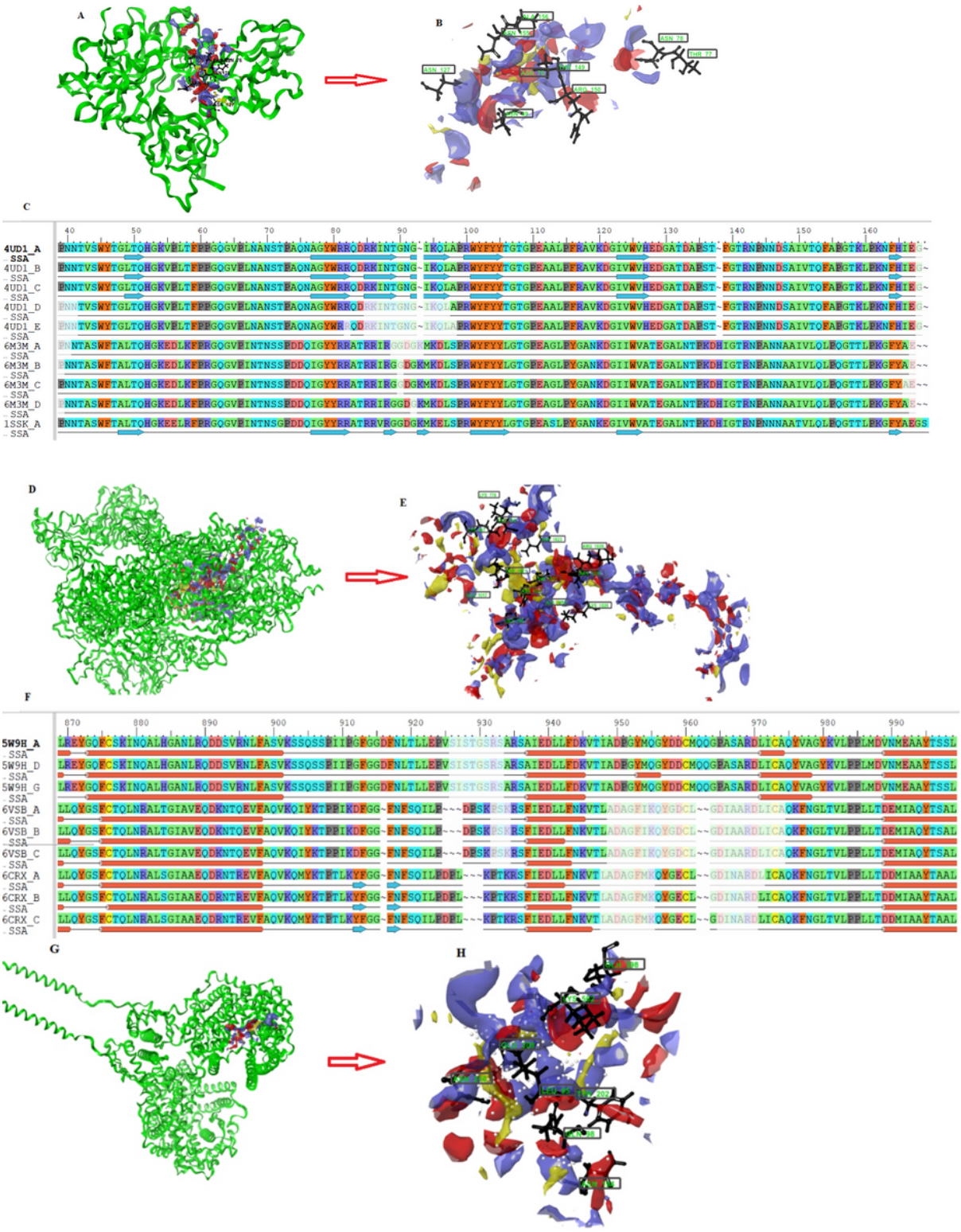

Figure 1

Binding site analysis of PDB 6M3M (A-C), PDB 6VSB (D-F) and PDB 6M17 (G-H): A-the structure of the nucleocapsid protein (green ribbon) with active binding site map (blue and red cartoon); B-the active residues (black ball and stick, green labels) within the binding site for drug-receptor interactions; C-the alignment of the NTD regions of the nucleocapsid phosphoproteins of SARS-CoV-2 (6M3M), SARS-CoV-1 (1SSK) and MERS-CoV (4UD1) within which the active residues are located. D-the structure of the spike

glycoprotein (green ribbon) with active binding site map (blue and red cartoon); E-the active residues (black ball and stick, green labels) within the binding site for drug-receptor interaction; F-the alignment of the spike glycoprotein structures of SARS-CoV-2 (6VSB), SARS-CoV-1 (6CRX) and MERS-CoV (5W9H), G-the human ACE2 structure (green ribbon) with active binding site map (blue and red cartoon); H-the active residues (black ball and stick, green labels) for drug-receptor interactions.

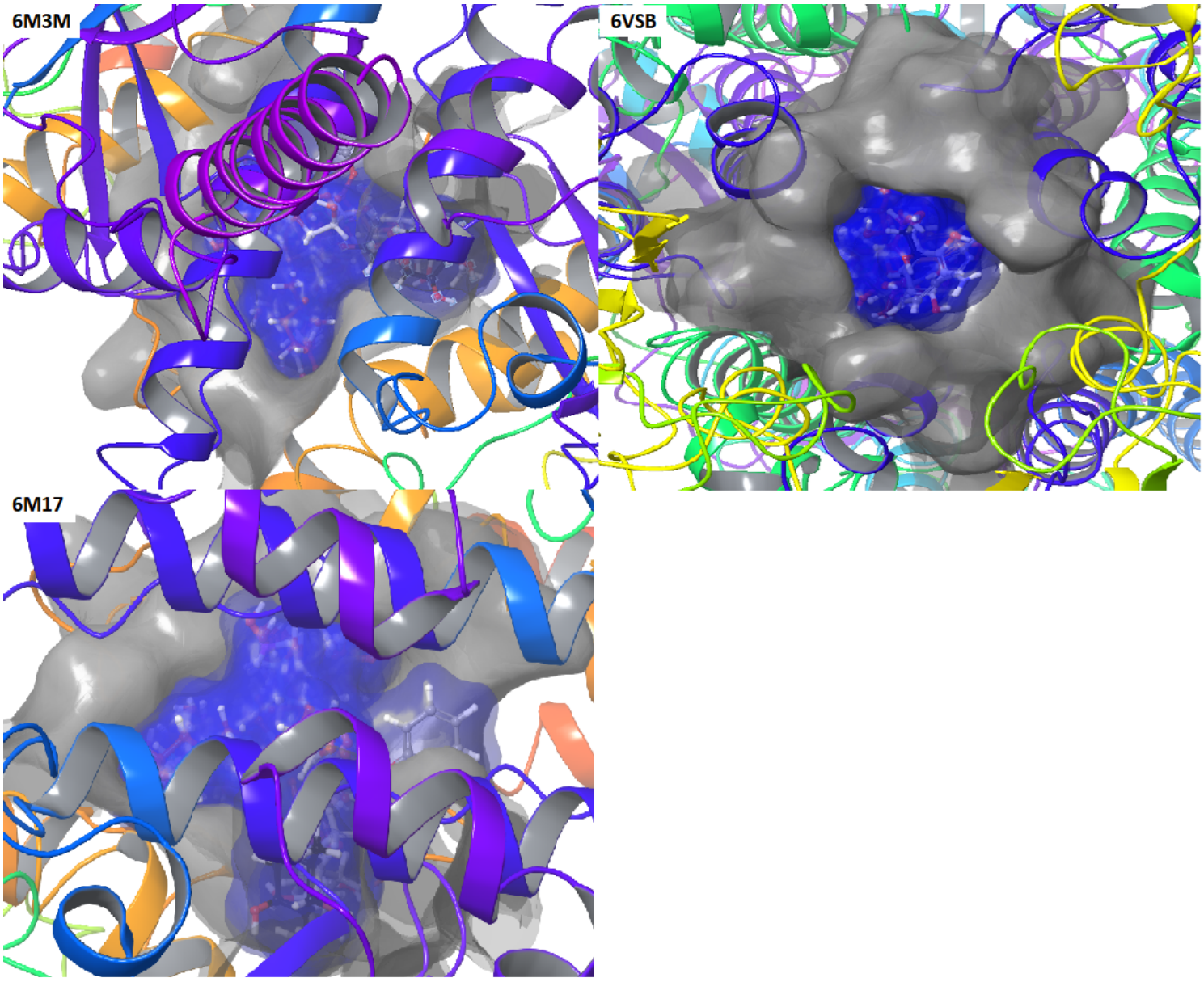

Figure 2

Surface structures of the selected drugs buried within the active binding sites of the targets represented by PDB: 6M3M, 6VSB and 6M17. All the drugs deeply occupy the same sub-site cavity of each receptor and this could infer good interactions and the possibility of similar biological functions.

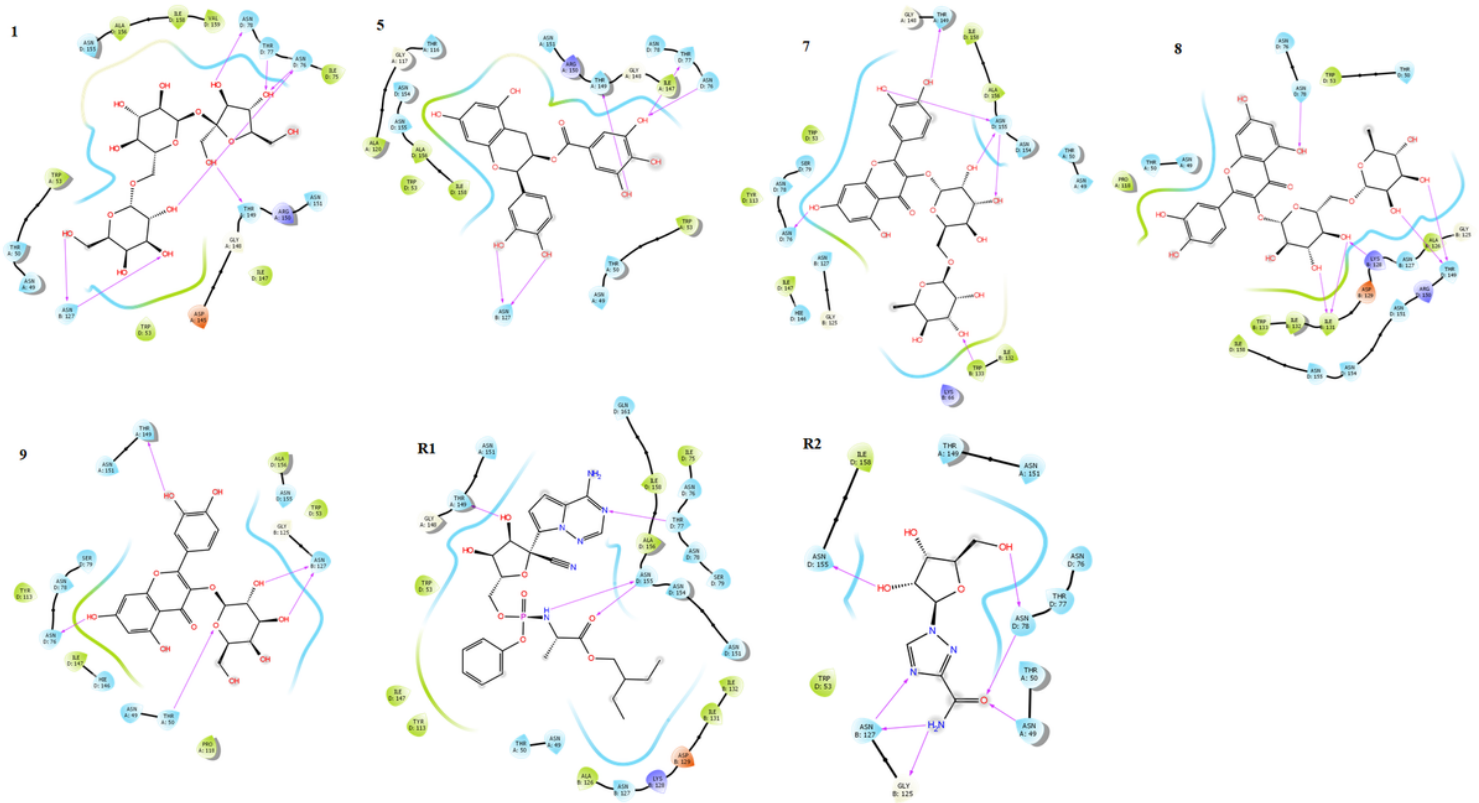

Figure 3

Binding poses of the selected drugs against PDB: 6M3M showing interactions of the selected drugs and the references with amino acid residues in the active cavity as hydrogen bonding (magenta arrow), π - cation (red line), salt bridge (blue line) and π - π stacking (green line).

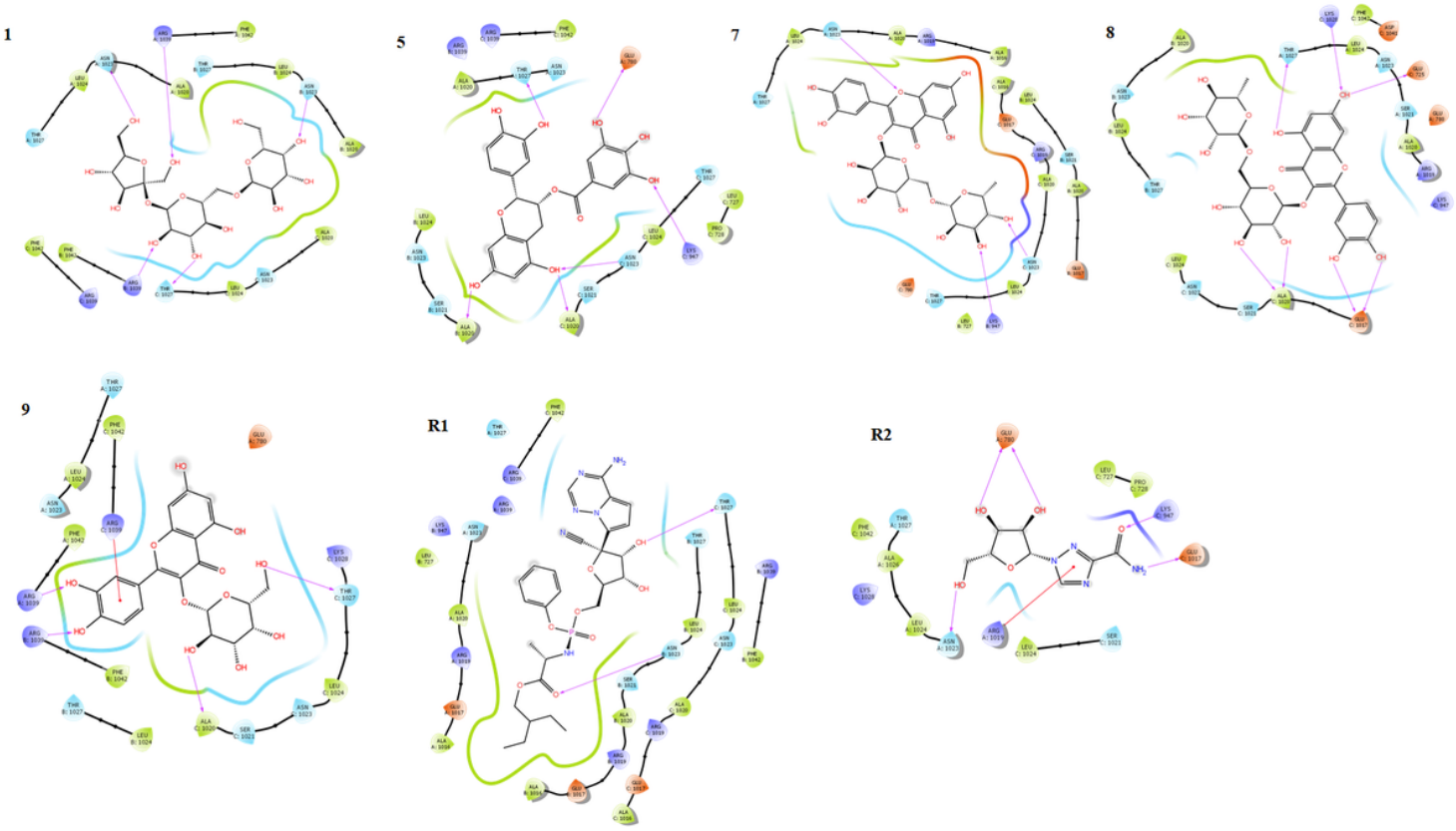

Figure 4

Binding poses of the selected drugs against PDB: 6VSB showing interactions of the selected drugs and the references with amino acid residues in the active cavity as hydrogen bonding (magenta arrow), π - cation (red line), salt bridge (blue line) and π - π stacking (green line).

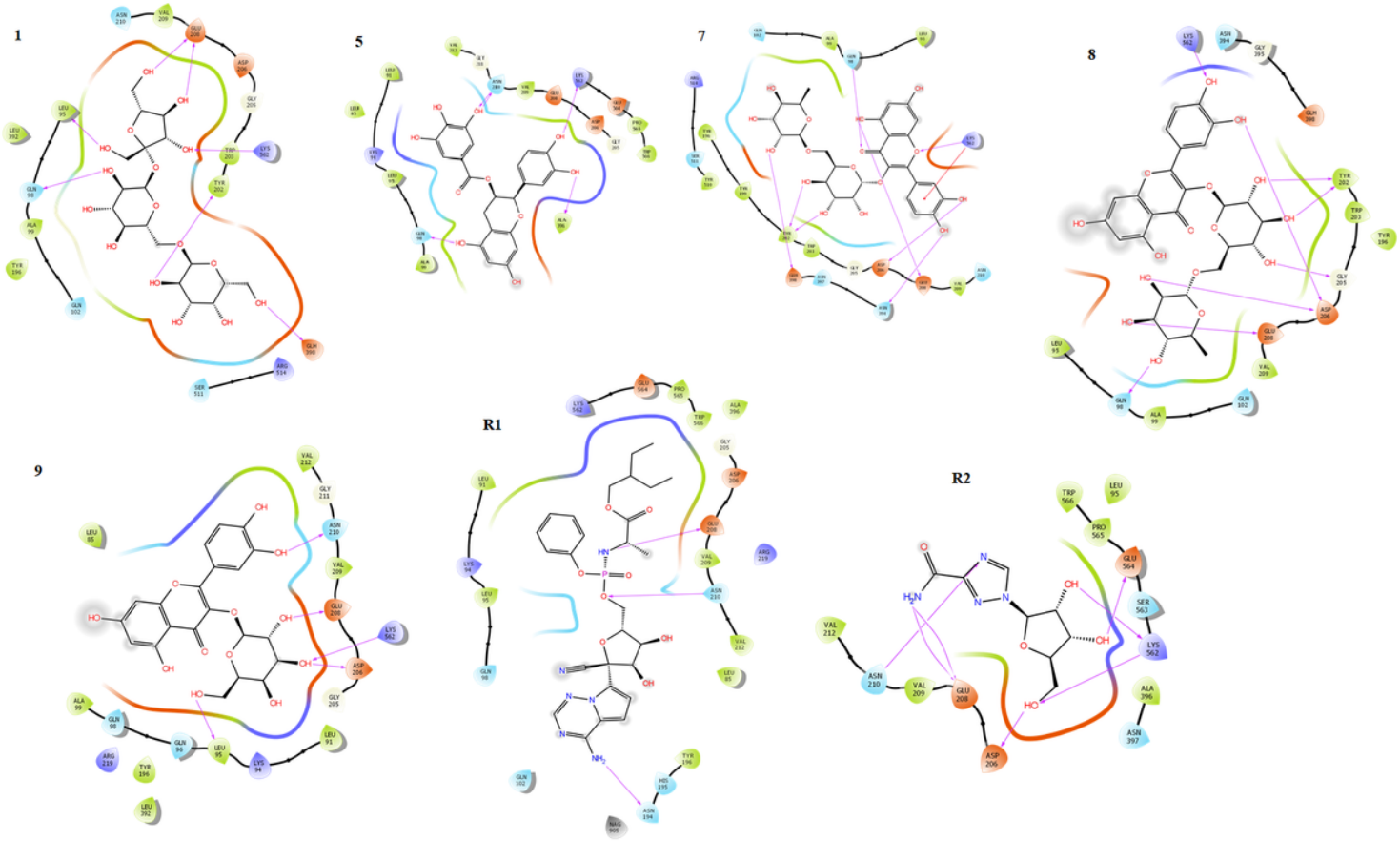

Figure 5

Binding poses of the selected drugs against PDB 6M17 showing interactions of the selected drugs and the references with amino acid residues in the active cavity as hydrogen bonding (magenta arrow), π - cation (red line), salt bridge (blue line) and π - π stacking (green line).

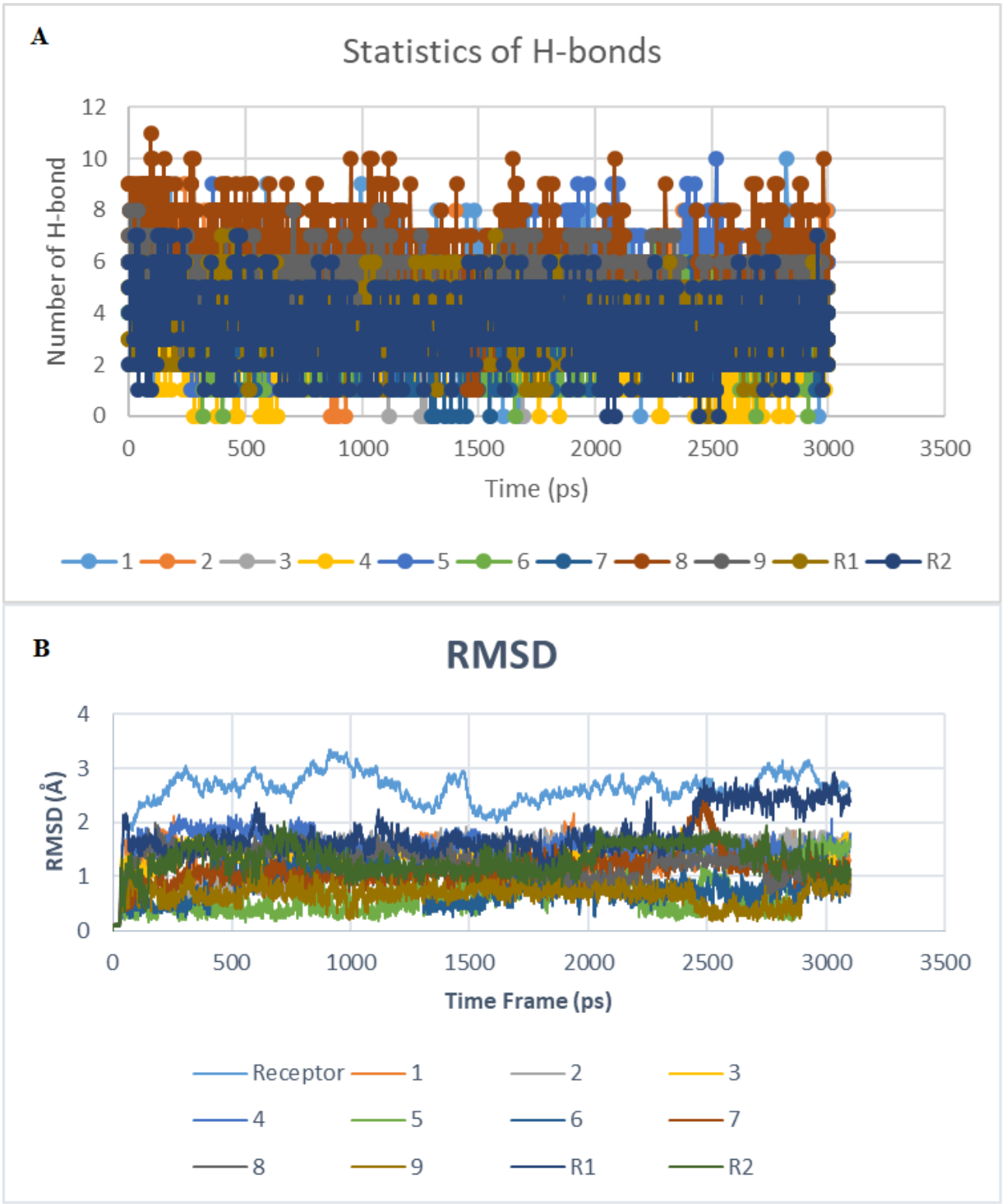

Figure 6

Molecular dynamics conformations for the selected drugs-6M3M complexes: (A) Hydrogen bond formation along the simulations of the selected drugs and the references with receptor within the period of 3000 ps. Stronger interactions are favoured by higher degrees of H-bond formation; (B) RMSD plot of the nine selected drugs, the references and receptor backbone. The lower the deviations from the mean point the more stable the system

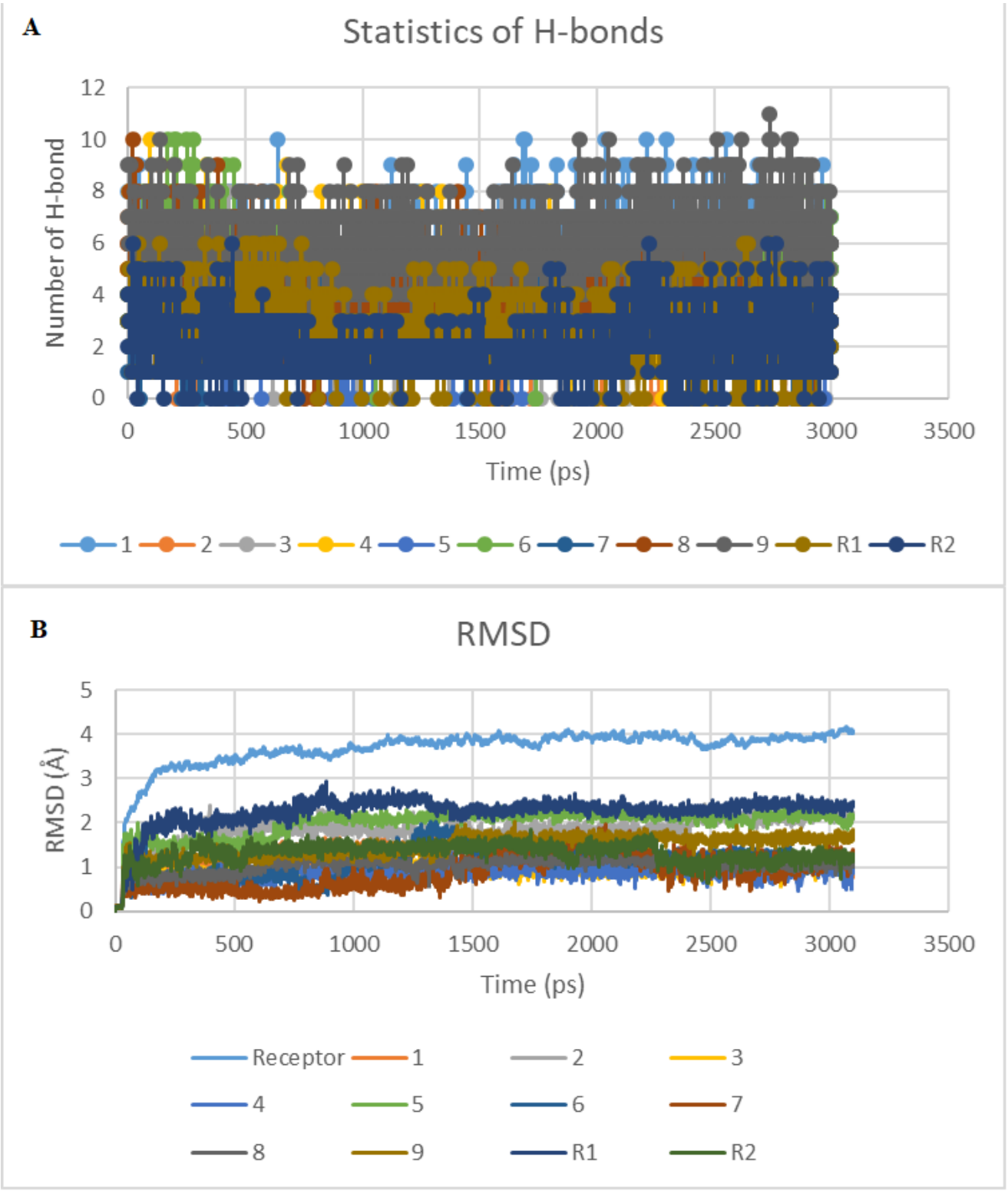

Figure 7

Molecular dynamics simulation results for the selected drugs-6VSB complexes: (A) Hydrogen bond formation along the simulations of the selected drugs and the references with receptor within the period of 3000 ps. Stronger interactions are favoured by higher degrees of H-bond formation; (B) RMSD plot of the nine selected drugs, the references and receptor backbone. The lower the deviations from the mean point the more stable the system

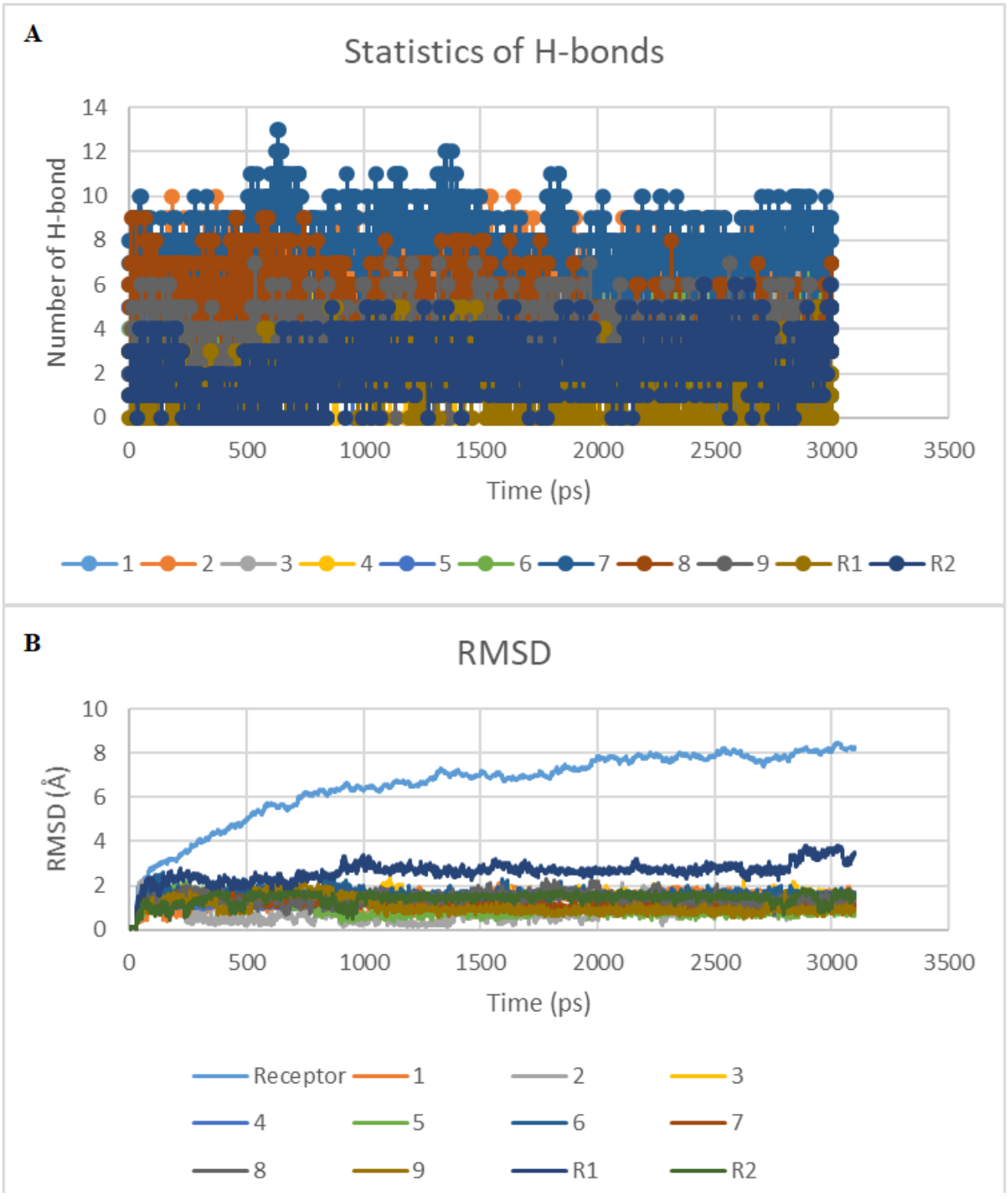

Figure 8

Molecular dynamics simulation results for the selected drugs-6M17 complexes: (A) Hydrogen bond formation along the simulations of the selected drugs and the references with receptor within the period of 3000 ps. Stronger interactions are favoured by higher degrees of H-bond formation; (B) RMSD plot of the nine selected drugs, the references and receptor backbone. The lower the deviations from the mean point the more stable the system